Mechanical & Materials Engineering Faculty Publications

Mechanical & Materials Engineering, Department of

2013

Elastic–Plastic Analysis and Strength Evaluation of Adhesive Joints in Wind Turbine Blades

Yi Hua
University of Nebraska–Lincoln, yhua3@unl.edu

Ananth Ram Mahanth Kasavajhala
University of Nebraska-Lincoln, arm13888@gmail.com

Linxia Gu
University of Nebraska - Lincoln, lgu2@unl.edu

Elastic–Plastic Analysis and Strength Evaluation of Adhesive Joints in Wind Turbine Blades

Yi Hua,[1] Ananth Ram Mahanth Kasavajhala,[1] and Linxia Gu[1, 2]

1. Department of Mechanical and Materials Engineering, University of Nebraska-Lincoln, Lincoln, NE 68588-0656, USA
2. Nebraska Center for Materials and Nanoscience, Lincoln, NE 68588-0656, USA

Corresponding author — Linxia Gu, Department of Mechanical and Materials Engineering, University of Nebraska-Lincoln, Lincoln, NE 68588-0656, USA; tel 402 472-7680, fax 402 472-1465, email lgu2@unl.edu

Abstract
The objective of this paper is to investigate the performance of adhesive joints of carbon/epoxy wind turbine blade subjected to combined bending and tension loadings through finite element method. The influence of adhesive material properties and geometrical details including fillet and imperfections was examined in terms of interlaminar stresses in the adhesive layer. The variation of stress intensity with change in adhesive shear modulus has also been investigated, while contour integral method was used for evaluating the stress intensity factors (SIF) at the imperfection tip. Furthermore, the strength of the joint was assessed through the crack initiation and propagation analysis. Results suggested that either adding a fillet or considering the plasticity led to the reduced peak stresses at the edge of the adhesive layer and redistributed the load to low stress regions. Inclusion of imperfections has resulted in high stress concentrations in the adhesive layer and reduction in the strength of the joint. Compared to the filleted adhesive, the strength of the joint reduced 2.4% and 4.8% considering a flat adhesive and filleted adhesive with through-thickness imperfection, respectively. Large shear modulus of the adhesive diminishes the fracture strength with the increased SIF.

Keywords: Laminates, Adhesion, Fracture, Finite element analysis (FEA), Wind turbine blade

1. Introduction

Polymer matrix composites have been extensively used in the construction of large-scale wind turbine blades due to the low weight and high stiffness requirements [1,2]. Composite blade and its supporting spars are usually manufactured in parts and then bonded together with adhesives. During a typical 20-year service life, adhesively bonded wind turbine blades are subjected to static and fatigue loads under various environmental conditions. Thus, there is a need for rigorous analysis of the stress states in adhesive joints to facilitate a better design for wind turbine blades [3–5]. Jensen et al. [6] has performed a static bending test of a 34 m composite wind turbine blade to failure under flap-wise loading conditions and simulated the whole process. Overgaard et al. [7,8] recently tested on a 25 m wind turbine blade to study the failure mechanism of the blades. The structural response to the applied bending loads and interlaminar failure were simulated to correlate with the experimental measurements. Samborsky et al. has reported the experimental results of over 250 static and fatigue tests of thick adhesive joint specimens prepared by a turbine blade manufacturer [9]. They have observed that crack initiated at the flaw areas in the adhesive, which led to unexpected structural response regarding the joint failure and its associated strength [9,10]. These existing researches focused on the global behavior of the turbine blade, such as spar deflection, blade stiffness and stress levels. Since wind turbine blades are large-scale structures, it is difficult to avoid flaws in the manufacturing process, such as air bubbles in the adhesive layers. Detailed local characterization and analysis, such as geometric imperfections and its associated stress intensity behaviors, are lacking due to the computational difficulty for accurate predictions [6,11–15].

In this work, detailed finite element model of the spar–shell assembly has been developed to investigate the performance of carbon/epoxy wind turbine blade. The influence of material and geometrical properties is examined in terms of interlaminar stresses. The variation of stress intensity with change in adhesive shear modulus has been investigated, while contour integral method is used for evaluating the stress intensity factors (SIF) K_I, K_{II} and K_{III} at the flaw tip. Furthermore, the analysis of crack initiation and propagation behavior is also used to evaluate the strength of the adhesive joint.

2. Finite element modeling

A schematic sketch of a wind turbine blade was shown in the left panel of Figure 1. The composite shell is supported by the spars to prevent the structural bucking of the blade. The spar and aerodynamic shell are glued together [16]. A three-
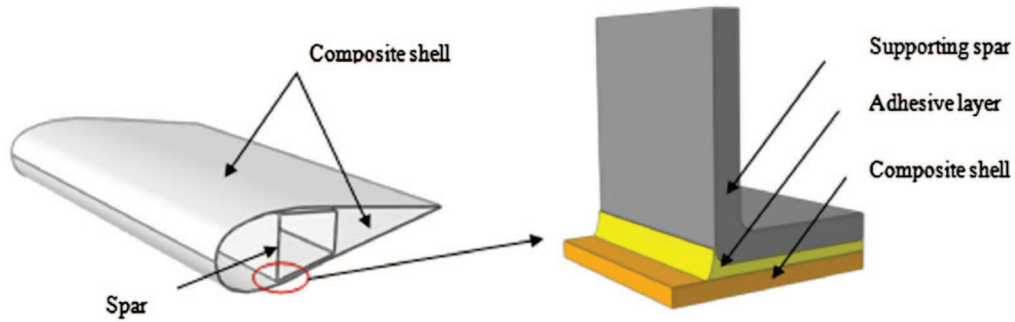
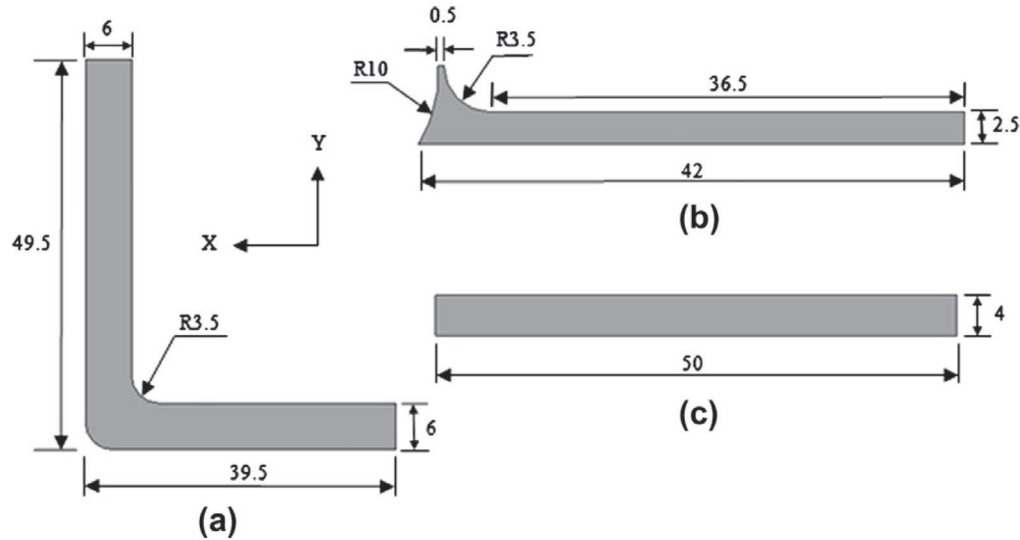**Figure 1.** Solid model of the adhesive joint for wind turbine blade.

Figure 2. Dimensions of (a) supporting spar, (b) adhesive layer and (c) composite shell.

Table 1. Material properties of carbon/epoxy composite and FM73 adhesive [17].

Properties	Carbon/epoxy	FM73 adhesive
Longitudinal modulus E_1 (GPa)	145	1.1
Transverse in-plane modulus E_2 (GPa)	10	–
Transverse out of plane modulus E_3 (GPa)	10	–
In-plane shear modulus G_{12} (GPa)	7	0.382
Out of plane shear modulus G_{13} (GPa)	7	–
Out of plane shear modulus G_{23} (GPa)	3.7	–
Major in-plane Poisson's ratio ν_{12}	0.25	0.44
Major out of plane Poisson's ratio ν_{13}	0.25	–
Major out of plane Poisson's ratio ν_{23}	0.5	–
Density (g/cm^3) 1.6	1.6	1.2
Fracture energy (kJ/m^2)	–	2

dimensional model of the adhesive joint between the composite shell and load-carrying spar was then developed using commercial finite element software ABAQUS (Dassault Systems Simulia Corp., RI, USA). The dimensions of the supporting spar, adhesive layer and composite shell are as depicted in Figure 2. The supporting spar is adopted as 1.5 times thicker than the composite shell so as to increase the strength of the support. Carbon/epoxy laminates with 4 plies (orientation 0°/+45°/–45°/0°) and 6 plies (orientation 0°/+45°/90°/90°/–45°/0°) have been used for the composite shell and spar material, respectively. Structural adhesive FM73 is used as bonding material with the isotropic elastic modulus of 1.1 GPa. The material properties are summarized in Table 1.

The model is meshed with reduced 8-node hexahedral elements (C3D8R). The mesh size was chosen as 1.0 mm through a mesh convergence study. The loading condition is to simulate a full scale wind turbine blade subjected to the lifting and drag force resulted from wind-induced pressure differences [16]. The composite shell is constrained in all degrees of freedom while 100 MPa of loading along y-direction combined with a 3 mm displacement along negative x-direction, is applied on the far end of supporting spar. Perfect adhesion is assumed on the interfaces between adhesive layer with composite shell or spar. SIF at the crack tip in the adhesive layer are calculated using contour integral method [18]. Furthermore, the extended finite element method (XFEM) [19,20] coupled with cohesive traction separation law has been used to model crack initiation and propagation in the adhesive layer.

3. Results and discussions

In this work, the interlaminar stresses, including peel stress S22 and shear stresses S12 and S23, in the adhesive layer are evaluated along six different paths in the higher stress region (Figure 3). The distance along y-direction from 0 to 2.5 mm represents the adhesive layer in paths 3–6. However, due to the nonlinearity in geometry (fillet in the adhesive), the adhesive thickness in path-1 extends up to 6 mm while it is 3 mm in path-2.

3.1. Effect of adhesive plasticity

Elastic material model is usually used to represent the response of the adhesive layer in the joint analysis [9]. The plasticity of the adhesive is considered here. A linear hardening
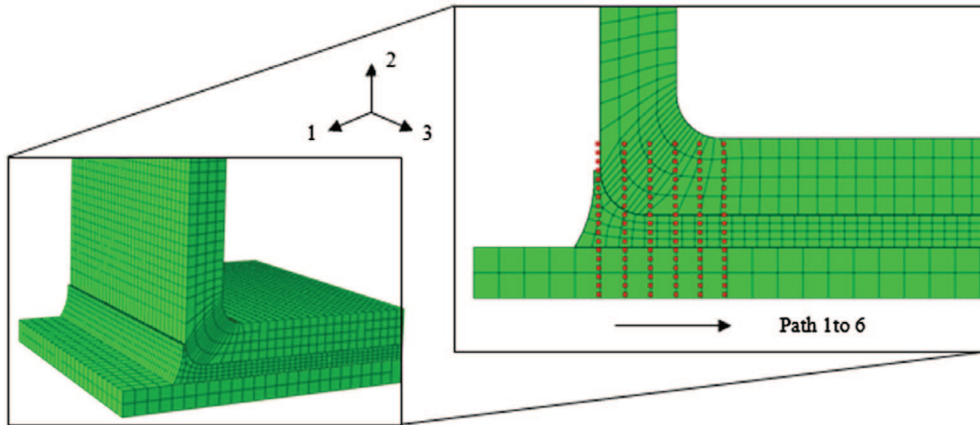
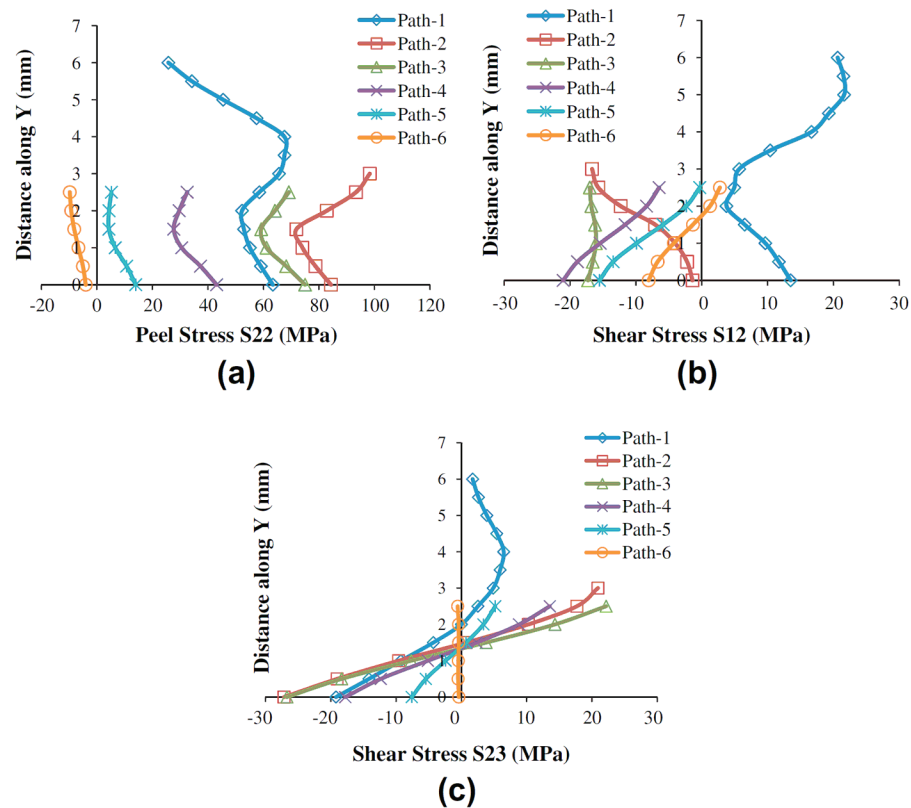**Figure 3.** Paths in the higher stress region of the joint.

Figure 4. Distribution of (a) peel stress S22, (b) shear stress S12 and (c) shear stress S23 along six paths for pure elastic adhesive.

material model of the adhesive layer is adopted with yield strength of 40 MPa and hardening coefficient of 1 GPa [21]. The distributions of interlaminar stresses along paths 1–6 for elastic adhesive are depicted in Figure 4, which served as the baseline data. The relative differences of these interlaminar stresses for adhesive material with and without plasticity are shown in Figure 5. It is clear that plasticity redistributes load and relieves stress concentrations in the adhesive layer. There is 8.2% reduction in the maximum peel stress considering the plasticity of the adhesive. As path number increases, a relative shift from tension to compressive peel stresses is observed in the adhesive layer due to bending load. The shear stress S23 changes its sign in the middle layer. The path by path comparison has shown that peel stress increases beyond path-3 after considering the plasticity of the adhesive. This indicates that the alleviated stresses in the high stress region are at the ex-

pense of load redistribution. Moreover, the maximum shear stress has been reduced by 4.6% and 13.3% for S12 and S23, respectively. Regardless of plasticity of the adhesive, large shear stress at the tip of adhesive layer could cause mode-II fracture of the joint.

3.2. Effect of adhesive fillet

Adhesive layer plays a vital role in transmitting load from the composite shell to the supporting spar. The geometrical features such as fillet could affect the mechanical strength of the adhesive joint. Figure 6 shows the relative difference of interlaminar stresses along paths 1–6 in the adhesive with and without fillet. It is noted that all interlaminar stresses in the adhesive layer increase its magnitude except shear stress S12 decreases along path-1. The effect of fillet on the interlam-
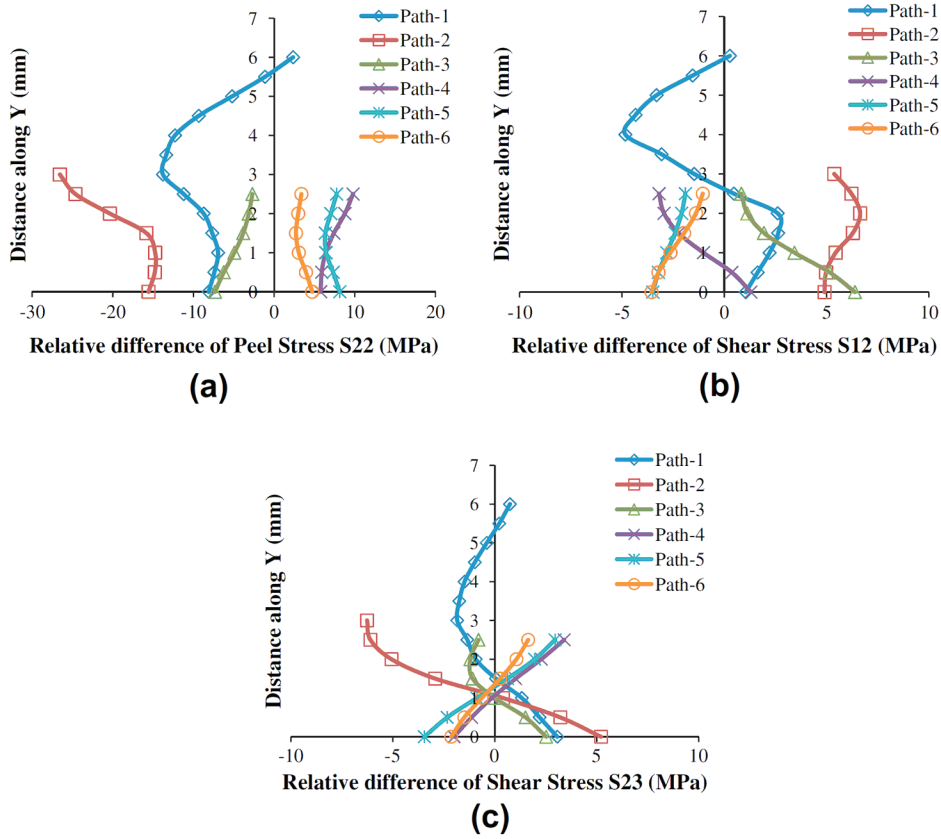
Figure 5. Relative difference of (a) peel stress S22, (b) shear stress S12 and (c) shear stress S23 along six paths for adhesive with plasticity.
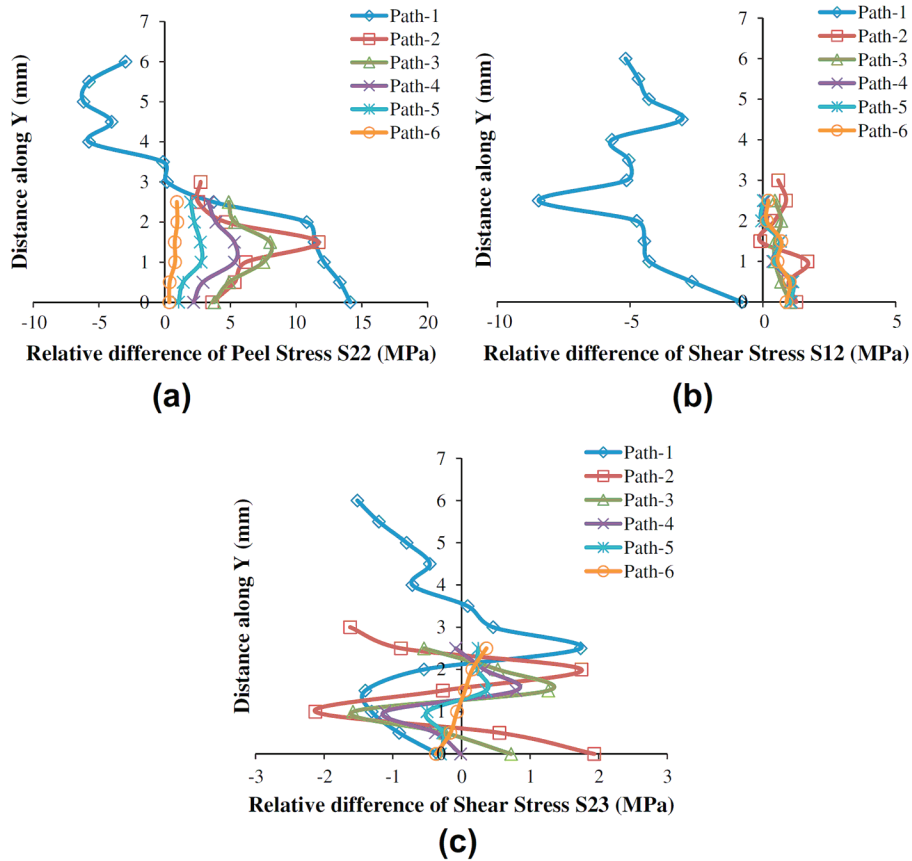

Figure 6. Relative difference of (a) peel stress S22, (b) shear stress S12 and (c) shear stress S23 along six paths for flat adhesive.
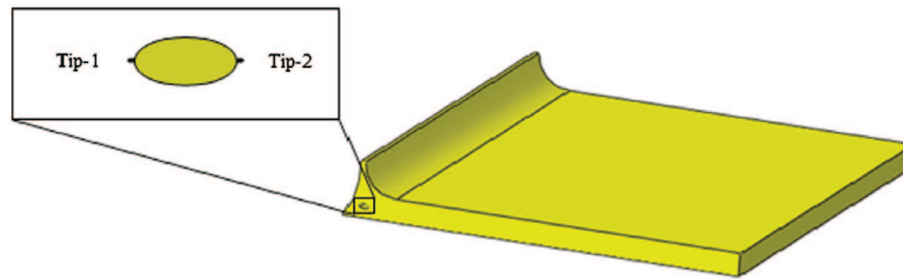
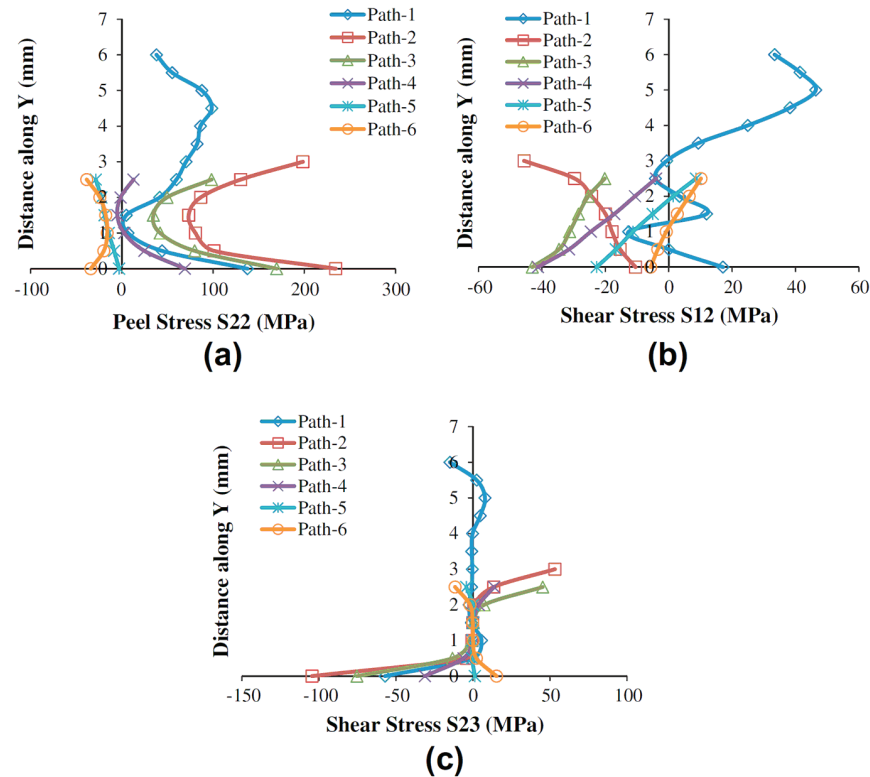**Figure 7.** Adhesive layer with a through-thickness elliptic cylinder.

Figure 8. Distribution of (a) peel stress S22, (b) shear stress S12 and (c) shear stress S23 along six paths for filleted adhesive with through-thickness imperfection.

inar stresses in the adhesive layer generally reduced as path number increases, i.e. away from the fillet edge. This indicates that a fillet impacts local stress concentrations. Absence of fillet leads to 3.0% increase in maximum value of peel stress in the adhesive layer while shear stresses S12 and S23 decrease by 6.5% and 4.6%, respectively. This is in total agreement with experimental results obtained by Adams et al. [22].

3.3. Effect of through-thickness imperfection

It is unavoidable that the imperfections exist in the adhesive layer because of entrapped air bubbles [23]. To investigate the effect of imperfection, a through-thickness elliptic cylinder (1 mm by 0.5 mm) positioned at 1.25 mm away from the adhesive tip (Path-1) is added to the model as shown in Figure 7. The resulting stress distribution along paths 1–6 in the adhesive joint is depicted in Figure 8. It is obvious that inclusion of imperfection has resulted in increased stress concentrations in the adhesive layer. The maximum peel stress S22 and shear stresses S12 and S23 in the adhesive layer increased by 2.29, 2.22 and 2.65 times, respectively. The peak peel stress in the adhesive layer has shifted to the adhesive–shell interface instead of adhesive–spar interface in case of without imper-

fections. It is clear that stress states in the adhesive layer are sensitive to imperfection, which is consistent with the observations by Guo et al. [23].

Fracture is commonly initiated from region with defects. To assess the stability of the adhesive joint with elliptical void, SIF are computed at the two tips of the void, referred as tip-1 and tip-2 (Figure 7). The resultant mode-I, mode-II and mode-III SIF at both tips are plotted with respect to the shear modulus of the adhesive as shown in Figure 9. It is clear that mode-I and mode-II are the more dominant modes with mode-I leading the way. This agrees with the experimental observation by Samborsky et al. [9]. The mode-I SIF variation between the two void tips is 19.5% at the 2000 MPa shear modulus, while in mode-II SIF the difference is 71%. Our results also show that the SIF increase with the larger adhesive shear modulus causing delamination or breakage. However, lower shear modulus reduces the bonding strength.

3.4. Crack initiation and propagation

The crack initiation and propagation are captured using the XFEM through a built-in user subroutine UEL_XFEM. Instead of embedding a crack tip in the adhesive, the XFEM automati-
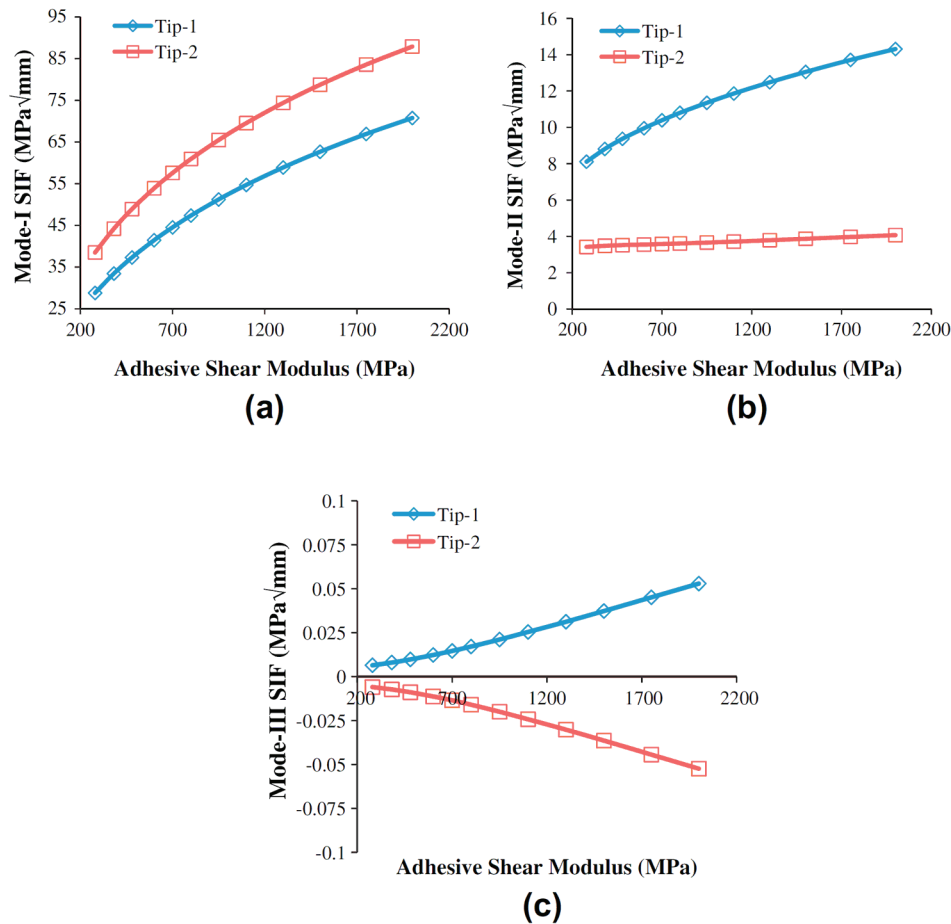
Figure 9. Variation of (a) mode-I SIF, (b) mode-II SIF and (c) mode-III SIF in the filleted adhesive layer.

cally introduces a new cohesive segment in the predefined enrichment nodes when the critical cohesive traction is reached. Cracks are introduced as jumps in the displacement fields, with their magnitude governed by the cohesive traction separation constitutive law [18,20]. The fracture behaviors of adhesive joints, including flat adhesive as well as filleted adhesive with and without throughthickness imperfection were investigated in this work. The maximum principal stress of 50 MPa is used to control the initiation of crack. The fracture energy release rate is specified as 2 N/mm. In all three cases, cracks are found to initiate in the upper portion of the adhesive layer and propagate following a path immediately adjacent to the adhesive–spar interface till they reach at the adhesive–spar interface. The delamination at the interface is not considered in the current study. In this work, the load at the time of crack initiation is used to assess the strength of adhesive joints, which is observed as 31.5 MPa for filleted adhesive with through-thickness imperfection, compared to the 32.3 MPa for flat adhesive, and 33.1 MPa for filleted adhesive joint without imperfections. It is clear the strength of the adhesive joint reduces 2.4% and 4.8% considering a flat adhesive and filleted adhesive with throughthickness imperfection, respectively.

4. Conclusions

Finite element method has been used to study the performance of the carbon/epoxy spar–shell assembly in a wind turbine blade subjected to bending. The effects of material and geometrical properties of the adhesive layer including void

are investigated. Crack initiation and propagation behavior is used to evaluate the strength of the adhesive composite joint. The conclusions are summarized as following:

- Considering the plasticity of the adhesive material, there is 8.2% reduction in the maximum peel stress while the maximum shear stress has been reduced by 4.6% and 13.3% for interlaminar shear stresses S12 and S23, respectively.
- Both adding a fillet and considering the plasticity will reduce the peak stress concentrations at the edge of the adhesive layer and redistribute the load to low stress regions.
- Voids in the adhesive will lead to reduced joint strength with earlier crack initiation. There is more than two-fold increase in the magnitude of interlaminar stresses in the adhesive layer with one through-thickness imperfection.
- Large shear modulus of the adhesive usually improves the bonding strength, but diminishes the fracture strength with the increased SIF.

References

[1] Shokrieh MM, Rafiee R. Simulation of fatigue failure in a full composite wind turbine blade. Compos Struct 2006;74(3):332–42.

[2] Edwards KL. A brief insight into the selection and use of engineering adhesives for preliminary joint design. Mater Des 1998;19(3):121–3.

[3] Kong C, Choi S, Park H. Investigation on design for a 500W wind turbine composite blade considering impact damage. Adv Compos Mater 2011;20(2):105–23.

[4] Schubel PJ, Hutchinson JR, Warrior NA. A cost and performance comparison of LRTM and VI for the manufacture of large scale wind turbine blades. Renew Energy 2011;36(2):866–71.

[5] da Costa Mattos HS, Monteiro AH, Palazzetti R. Failure analysis of adhesively bonded joints in composite materials. Mater Des 2012;33(0):242–7.

[6] Jensen FM et al. Structural testing and numerical simulation of a 34 m composite wind turbine blade. Compos Struct 2006;76(1–2):52–61.

[7] Overgaard LCT, Lund E, Thomsen OT. Structural collapse of a wind turbine blade. Part A: Static test and equivalent single layered models. Compos Part A – Appl Sci Manuf 2010;41(2):257–70.

[8] Overgaard LCT, Lund E. Structural collapse of a wind turbine blade part B: progressive interlaminar failure models. Compos Part A – Appl Sci Manuf 2010;41(2):271–83.

[9] Samborsky DD, Sears AT, Mandell JF. Static and fatigue testing of thick adhesive joints for wind turbine blades. In: ASME wind energy symposium. USA; 2009.

[10] Jiang WC, Fan QS, Gong JM. Optimization of welding joint between tower and bottom flange based on residual stress considerations in a wind turbine. Energy 2010;35(1):461–7.

[11] Bazilevs Y et al. 3D simulation of wind turbine rotors at full scale. Part I: Geometry modeling and aerodynamics. Int J Numer Method Fluids 2011;65(1–3):207–35.

[12] Steinbrecher G et al. Characterization of the mode I fracture energy of adhesive joints. Int J Adhes Adhes 2006;26(8):644–50.

[13] Yang QD, Thouless MD. Mixed-mode fracture analyses of plastically–deforming adhesive joints. Int J Fract 2001;110(2):175–87.

[14] Guo YJ, Weitsman YJ. A modified specimen for evaluating the mixed mode fracture toughness of adhesives. Int J Fract 2001;107(3):201–34.

[15] Ouinas D, et al. Progressive edge cracked aluminium plate repaired with adhesively bonded composite patch under full width disbond. Compos Part B: Eng 2012;43(2):805–11.

[16] Sørensen BF, Jacobsen TK. Joining structural parts of composite materials for large rotorblades. In: Proceedings of the 27th risø international symposium on materials science: polymer composite materials for wind power turbines. Denmark; 2006.

[17] Gu L, Kasavajhala ARM, Zhao S. Finite element analysis of cracks in aging aircraft structures with bonded composite-patch repairs. Compos Part B: Eng 2011;42(3):505–10.

[18] ABAQUS v6.10 documentation. Dassault Systèmes Simulia Corp., Providence, RI; 2011.

[19] Belytschko T, Black T. Elastic crack growth in finite elements with minimal remeshing. Int J Numer Method Eng 1999;45(5):601–20.

[20] Giner E et al. An Abaqus implementation of the extended finite element method. Eng Fract Mech 2009;76(3):347–68.

[21] Kumar S, Pandey PC. Fatigue life prediction of adhesively bonded single lap joints. Int J Adhes Adhes 2011;31(1):43–7.

[22] Adams Robert D, Comyn J, Wake WC. Struct Adhes Joints Eng 1997:359.

[23] Guo YC, et al. The influence of hollow imperfections of adhesive on performances of interface of RC beams strengthened with HFRP. In AIP conference proceedings; 2010.